JOURNAL OF MATERIALS SCIENCE **37** (2002) 2331 – 2339

The development of microstructural and electrical characteristics in some thick-film resistors during firing

M. HROVAT, Z. SAMARDŽIJA, J. HOLC
Jožef Stefan Institute, Jamova 39, 1000 Ljubljana, Slovenia
E-mail: marko.hrovat@ijs.si

D. BELAVIČ*
HIPOT, Trubarjeva 7, 8310 Šentjernej, Slovenia

The development of microstructural and electrical characteristics (sheet resistivities, TCRs, and noise indices) in some thick-film resistors during the firing process has been evaluated. Three 1 kohm/sq. resistor pastes (Du Pont), based on RuO_2, ruthenate or a mixture of both conductive phases, were fired at temperatures from 500°C to 950°C. The cell parameters of the RuO_2 in the 8031 and the 2031 resistors, the bismuth ruthenate in the 8029 resistors and the lead ruthenate in the 2031 resistors, were calculated from X-ray data. Microstructures were analyzed by SEM and EDS microanalysis. The absolute values of the cold and hot TCRs first decreased to a minimum at 850°C and then increased again with increasing firing temperature. The noise indices of the resistors generally decrease with increasing firing temperature.

1. Introduction

Thick-film resistors consist basically of conducting phase, glass phase and organic vehicle; the last of these burns out during the high-temperature processing. In most modern resistor compositions the conductive phase is either RuO_2 or ruthenates. In addition, some other oxides are added either as modifiers of the temperature coefficient of resistivity (TCR) or modifiers of the temperature coefficient of expansion of the glass phase [1–3]. The main "requirements" for thick-film resistors are long-term stability, relatively narrow tolerances of the sheet resistivities after firing, and a low TCR. During firing, resistors reach the highest temperature (typically 850°C) in 10 or 20 min. and are only a relatively short time (typically 10 min) at the highest temperature. During the firing cycle the constituents of the material react with each other. The main change during firing is the transition from a mixture of glass grains and usually, much finer grains of conductive phase in a thick-film paste into conductive chains through the sintered glass in the fired resistor. The reactions presumably do not reach equilibrium, so the characteristics of the fired materials are a consequence of this frozen non-equilibrium [4, 5].

The development of electrical and microstructural characteristics during firing was studied either on model systems, i.e. a mixture of conductive and glass phase [3, 6–8] or with commercial thick-film resistors [9–12]. In most cases the sheet resistivity first decreases and then increases with increasing firing temperature, while the TCR (at least for RuO_2-based resistors) first increases and then decreases. This can be explained in simple terms as follows: the glass phase starts to sinter at 500°C to 600°C but at first this does not wet the conductive particles. The particles are "pushed" together which results in decreasing resistivity and, due to the high positive TCR of the RuO_2 [3], an increasing TCR. At higher temperatures the glass wets and "breaks up" agglomerates of the conductive particles which leads to increasing resistivity and decreasing TCR. These stages can sometimes overlap so that smooth changes of resistivity and TCR values vs. firing temperature can be observed. The dependence of sheet resistivity and TCR vs. firing temperature is schematically shown in Fig. 1 (after [12]). The aim of manufacturers of thick-film resistor materials is, however, to obtain the desirable characteristics for resistors fired in the production of thick-film hybrid circuits at 850°C. This is accomplished by optimizing the glass composition, by selecting the ratio of the particle diameters of the glass and conductive phase, and by adding the correct amount of modifiers.

The aim of this work is to gain some insight into the development of the thick-film resistor's electrical characteristics, i.e. sheet resistivity, TCR and noise, during the firing process. 1 kohm/sq. resistors from the Du Pont resistor series HS-80 (HS-8029 and 8031) and 2000 (2031) were evaluated. HS-80 is a relatively old and "well established" resistor series from the mid-1980s. The 2000 series was developed in the first half of the nineties with the aim of making possible the fabrication of small-size thick-film resistors with improved electrical characteristics aswell as a wider technology window, e.g. relatively insensitive to firing time or temperature and conductor metallurgy [13]. TCRs of

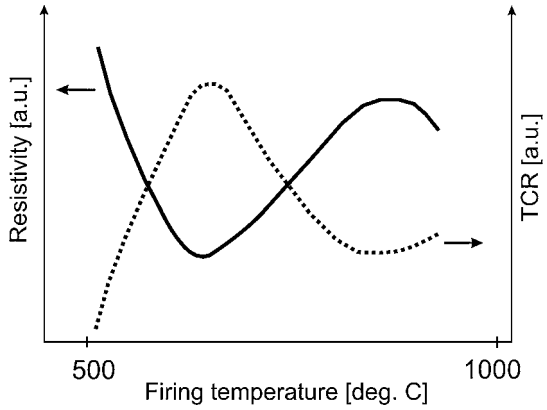

Figure 1 Sheet resistivity and TCR vs. firing temperature (schematically) [12].

HS-80 and 2000 resistors are under 100×10^{-6}/K and 75×10^{-6}/K, respectively. The conductive phase in HS-8029 is ruthenate, presumably $Bi_2Ru_2O_7$, in HS-8031 it is RuO_2, and in 2031 a mixture of RuO_2 and ruthenate, presumably $Pb_2Ru_2O_{6.5}$, as no bismuth was detected by energy-dispersive X-ray analysis in fired resistors [14]. Resistors were fired at different temperatures from 500°C to 950°C, the last temperature being 100 K higher than the ordinary firing temperature.

2. Experimental

The 8029, 8031 and 2031 thick-film resistor pastes were printed on 96% alumina substrates, dried for 15 min at 150°C and fired for 10 min at temperatures from 600°C to 950°C. Firing temperatures are listed in Table II. Resistors were terminated by prefired Pd/Ag thick-film conductors. The dimensions of the resistors used for electrical characterisations were 1×1 mm^2. The dimensions of the resistors used for microstructural analysis and X-ray diffraction analysis, which were printed and fired without conductor terminations, were 8×8 mm^2.

A JEOL JSM 5800 scanning electron microscope (SEM) equipped with an energy-dispersive X-ray analyser (EDS) was used for overall microstructural and compositional analysis of the resistors which were printed and fired on alumina ceramics. Prior to analysis in the scanning electron microscope, the samples were coated with carbon to provide electrical conductivity and to avoid charging effects. Resistors were analysed by X-ray powder diffraction analysis (XRD) with a Philips PW 1710 X-ray diffractometer using Cu Kα radiation. X-ray spectra were measured from $2\,\Theta = 20°$ to $2\,\Theta = 70°$ in steps of 0.02°.

Sheet resistivities were measured as a function of the firing temperatures. Cold (from −25°C to 25°C) and hot (from 25°C to 125°C) TCRs were calculated from resistivity measurements at −25°C, 25°C, and 125°C. Current noise was measured in dB on 100 mW loaded resistors by the Quan Tech method [15] (Quan Tech Model 315-C).

3. Results and discussion

3.1. XRD, Microstructural and EDS Characterisation

As mentioned in the Introduction, the conductive phase in 8029 resistors is ruthenate, in 8031 resistors RuO_2, and in 2031 resistors a mixture of RuO_2 and ruthenate. However, the thick-film resistor materials from different resistor series differ not only in the chemistry of the conductive phase but also in the composition of the glass phase. The results of the EDS analysis of the glass phase in the thick-film resistors, fired at 850°C, are shown in Table I [14]. All glasses contain lead, silicon and aluminium oxides. Boron oxide, which is also present in the glass phase, cannot be detected in EDS spectra because of the low relative boron weight fraction in the glass and the strong absorption of the boron Kα line during EDS analysis in the glass matrix. However, most thick-film resistors use glasses with roughly equal proportions of PbO, SiO_2 and B_2O_3, as glasses rich in PbO, SiO_2 or B_2O_3 have high temperature expansion coefficients, high melting temperature or glass immiscibility, respectively [16]. Other elements, detected in minor quantities, differ for each resistor series.

The XRD spectra of dried (150°C, 15 min) and fired (850°C, 10 min) 8029, 8031 and 2031 resistors are shown in Figs 2 and 3, respectively. The spectra of

TABLE I Qualitative results of EDS microanalysis of elements detected in the glass phase of resistors [14]

Resistor	Main elements	Other elements detected
8029	Si, Pb, Al	Mn, Cu, V
8031	Si, Pb, Al	Ca, Zn, Mn
2031	Si, Pb, Al	Mg, Zn, Ca, Ba

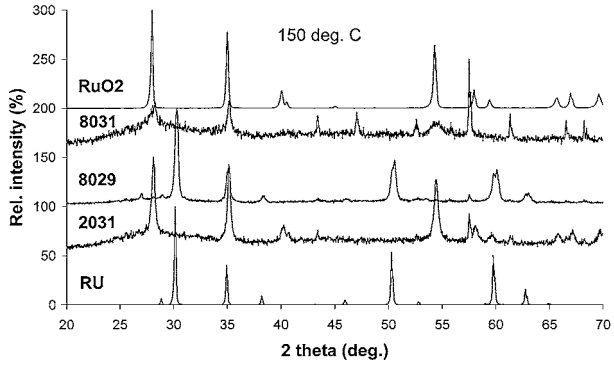

Figure 2 XRD spectra of 2031, 8029 and 8031 thick-film resistors, dried for 15 min at 150°C. Spectra of ruthenate (denoted RU) and of RuO_2 (denoted RuO_2) are also included.

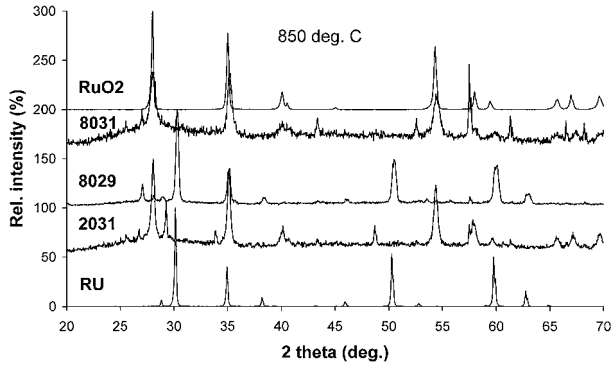

Figure 3 XRD spectra of 2031, 8029 and 8031 thick-film resistors, fired for 10 min at 850°C. Spectra of ruthenate (denoted RU) and of RuO_2 (denoted RuO_2) are also included.

ruthenate ($Pb_2Ru_2O_{6.5}$), denoted "RU" and of RuO_2, denoted "RuO_2", are also included in the graphs. The conductive phase in dried 2031 and 8031 resistors is based on ruthenium oxide and in 8029 on ruthenate. In the XRD spectrum of the 2031 resistor, after firing at 850°C, besides peaks of RuO_2, the peaks of ruthenate, shifted to smaller 2Θ values, also appeared. The position of peaks of the conductive phase, i.e. ruthenate in the 8029 resistor and RuO_2 in the 8031 resistor, is the same in resistors, dried at 150°C and resistors, fired at 850°C. The peak at $2\Theta \sim 27^\circ$ in the XRD spectra of the 8029 resistors can be attributed to the strongest (2 0 0) reflection at $2\Theta = 27.04^\circ$ of the $ZrSiO_4$ compound (JCPDS file 83-1383), which was also detected with EDS analysis in the microstructure of this resistor material. The relatively strong peak at around $2\Theta = 47.5^\circ$ in the spectrum of the 8031 resistor which was dried at 150°C disappears after firing at higher temperatures; its origins are not known. In the case of the 2031 resistors only peaks of RuO_2 are observed after drying at 150°C. Peaks of the ruthenate phase appeared after firing. Lead ruthenate is presumably formed from RuO_2 and PbO from the glass phase during firing.

The cell parameters of RuO_2 in the 8031 and 2031 resistors, bismuth ruthenate in the 8029 resistors and lead ruthenate in the 2031 resistors, were calculated from X-ray data. The number in the brackets indicates the accuracy of the last significant digit. Calculated

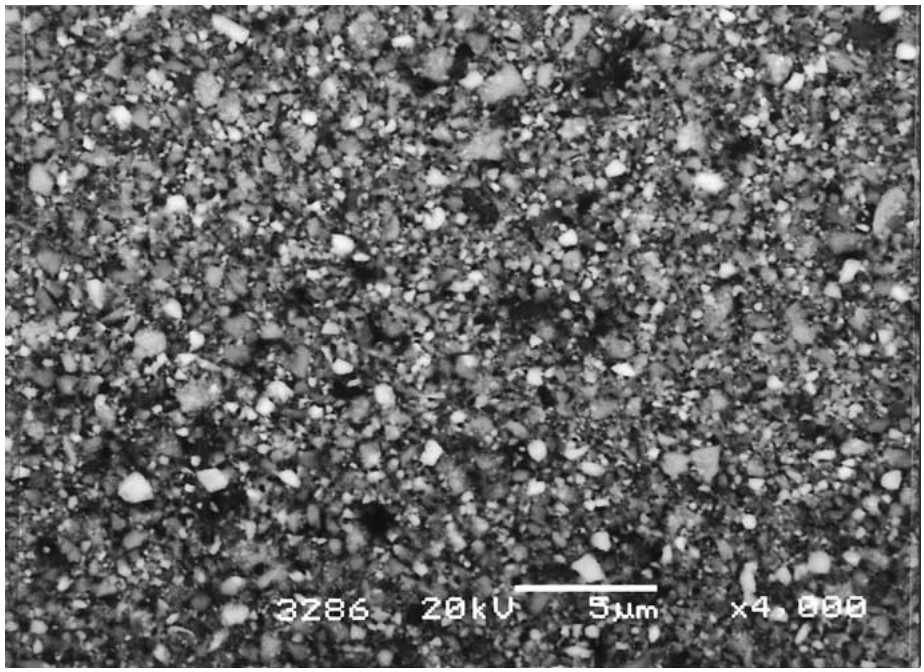

(a)

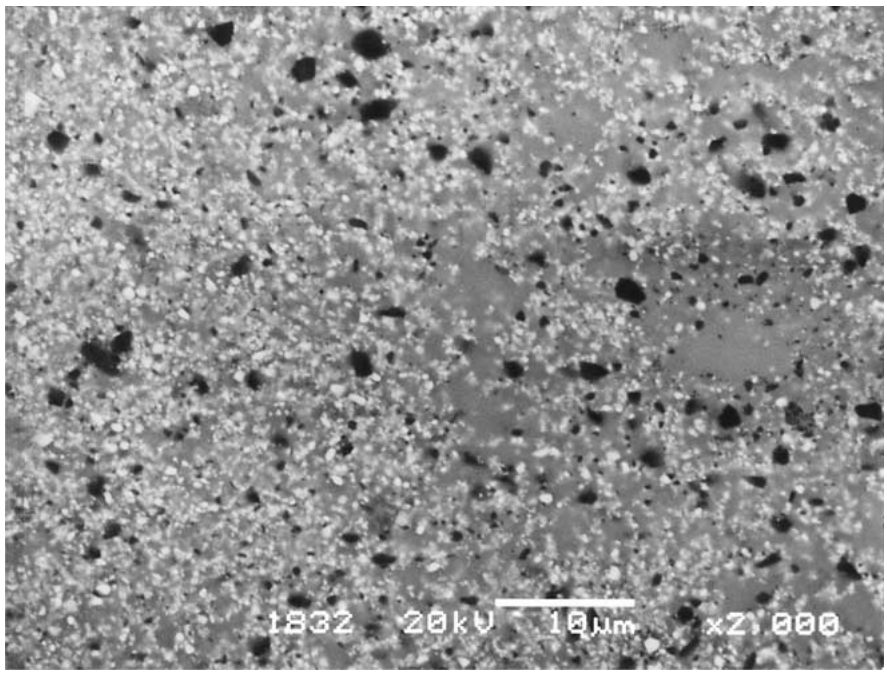

(b)

Figure 4 (a) Microstructure of thick-film resistor paste 8029, dried for 15 min at 150°C. (b) Microstructure of thick-film resistor 8029, fired for 10 min at 850°C. Light particles are conductive phase and dark grains are $ZrSiO_4$.

cell dimensions for tetragonal RuO_2 in both 8031 and 2031 resistors are in good agreement with data from the RuO_2 JCPDS file 40-1290 ($a = 0.4499$ nm and $c = 0.3107$ nm). The calculated cell dimensions of the cubic $Bi_2Ru_2O_7$ in the 8029 resistor ($a = 1.0223(5)$ nm) are smaller than the cell parameters reported in the literature ($a = 1.0299$ nm) [17–19]. Morten *et al*. also observed a decrease of the $Bi_2Ru_2O_7$ unit-cell dimensions in the pyrochlore based thick-film resistors after firing [11]. They attributed this decrease to the partial exchange of bismuth ions in the pyrochlore structure with lead ions from the glass phase during firing. However, even if all the bismuth were to be exchanged for lead, i.e., if the ruthenate was $Pb_2Ru_2O_{6.5}$, the unit-cell parameter a will still be 1.025 nm. The additional decrease of the unit-cell dimension could be tentatively ascribed to the partial exchange of bismuth oxide with copper or manganese oxide (see qualitative glass composition of 8029 resistor in Table I) and the formation of either $Bi_{2-x}Cu_xRu_2O_{7-y}$ or $Bi_{2-x}Mn_xRu_2O_{7-y}$ solid solutions [20].

The calculated lattice parameter of the lead ruthenate ($a = 1.0578(3)$ nm) in the 2031 resistor is larger than that of the $Pb_2Ru_2O_{6.5}$ (JCPDS file 34-0471; $a = 1.0252$ nm). The compound is therefore probably a member of the pyrochlore series, which can be described by the general formula $Pb_2(Ru_{2-x}Pb_x)O_{6.5}$ [19]. The increase of the pyrochlore unit-cell

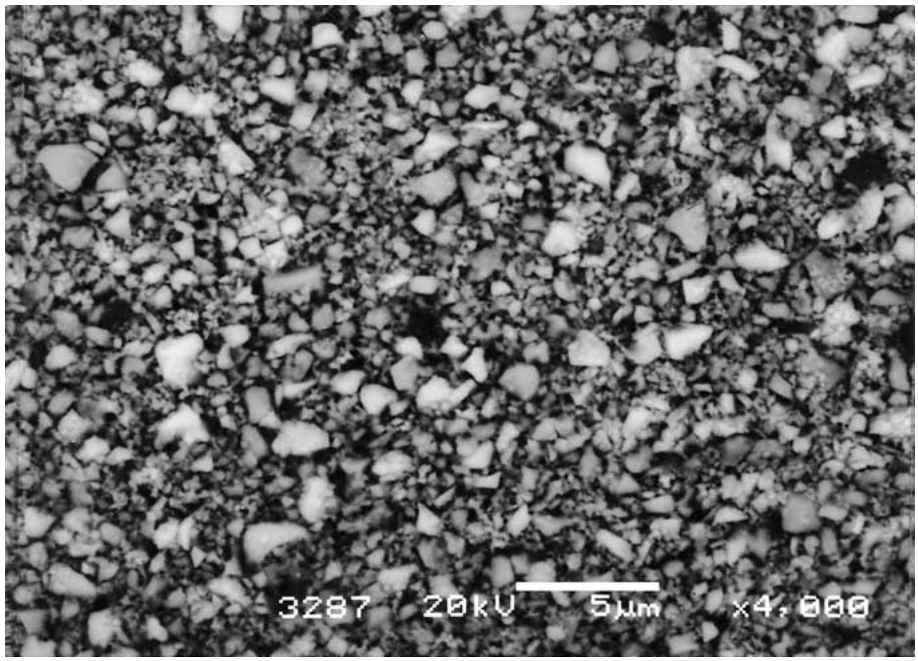

(a)

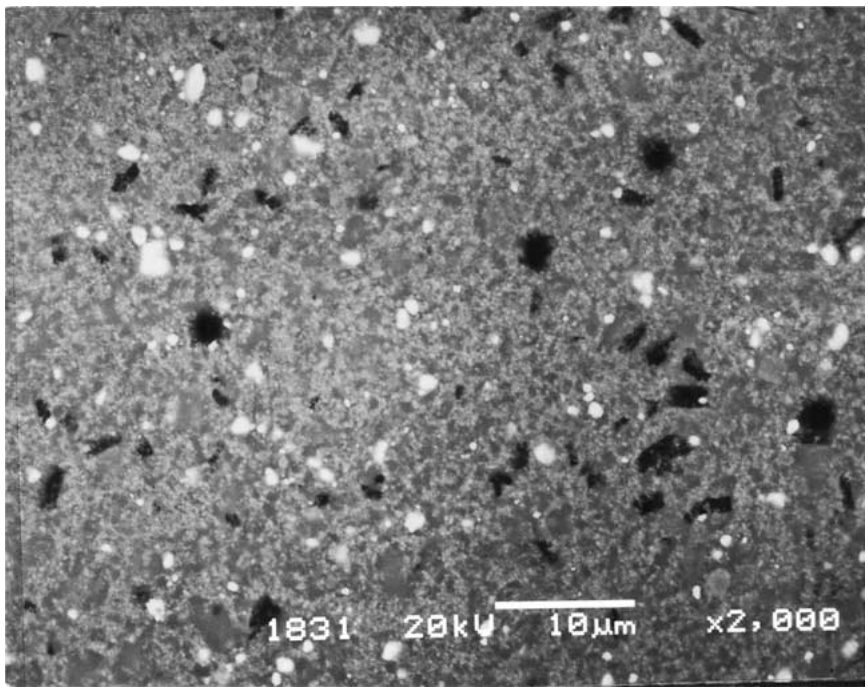

(b)

Figure 5 (a) Microstructure of thick-film resistor paste 8031, dried for 15 min at 150°C. (b) Microstructure of thick-film resistor 8029, fired for 10 min at 850°C.

dimensions is due to the substitution of larger Pb^{4+} ions (0.0775 nm) for Ru^{4+}ions (0.062 nm) on the B sites of the pyrochlore structure.

The microstructures of thick-film resistor pastes which were dried at 150°C and fired at 850°C are shown in Figs 4, 5 and 6 for 8029, 8031 and 2031, respectively. The resistor materials, which were dried at 150°C, have rather similar microstructures, mixtures of glass grains and much finer grains of conductive phase. Dark particles, observed in the 2031 resistors (Fig. 6a), are the glass phase which is rich in barium. After firing at 850°C all three resistor materials are densely sintered. The light particles are conductive phase, i.e. ruthenate in 8029, RuO_2 in 8031 and a mixture of ruthenate and RuO_2 in 2031. The dark particles in 8029 (Fig. 4b) and in 2031 (Fig. 6b) are $ZrSiO_4$, as determined by EDS microanalysis.

The microstructure of the 8031 resistor (Fig. 5b) consists of "chains" of lighter phase, the conductive clusters (very small RuO_2 particles embedded in glass) around glass "islands". The other two microstructures show a mixture of lighter particles of conductive phase in a glass phase. These microstructures correspond to two different types of thick-film resistor microstructures which are described in the literature [21–23]. The first type is characterized by the segregation of very

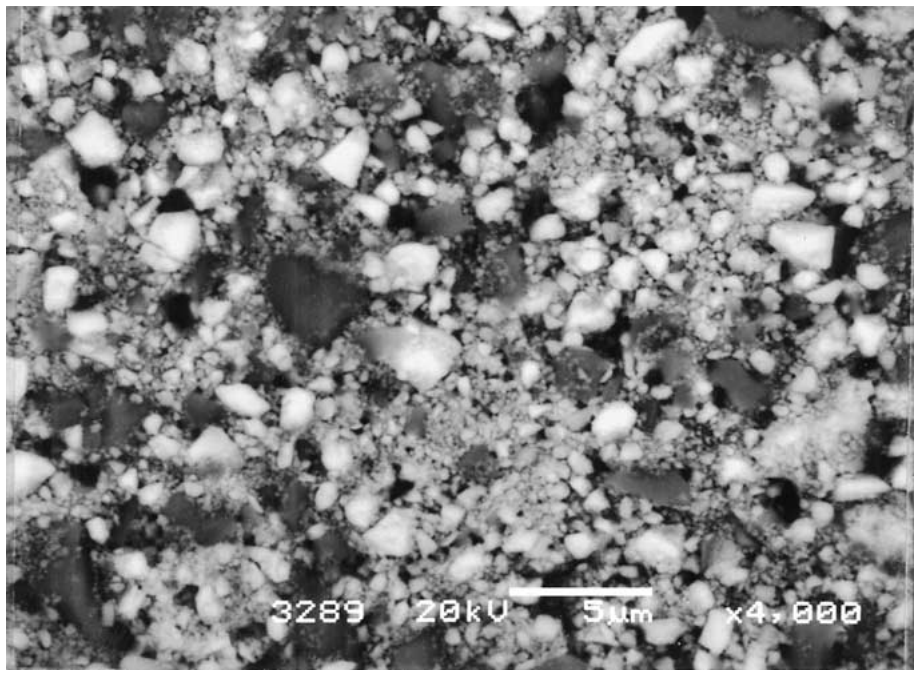

(a)

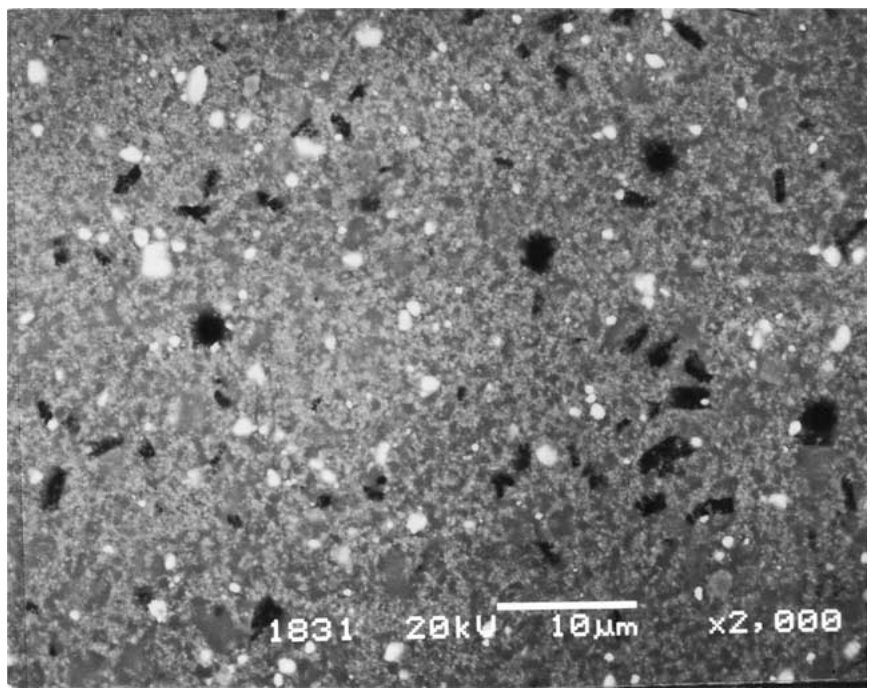

(b)

Figure 6 (a) Microstructure of thick-film resistor paste 2031, dried for 15 min at 150°C. Dark grains are the glass phase which is rich in barium. (b) Microstructure of thick-film resistor 2031, fired for 10 min at 850°C. Light particles are the conductive phase and dark grains are $ZrSiO_4$.

small conductive particles in "chains" around larger sintered glass grains and is associated with RuO_2-based resistors. The second type is a more or less homogenous mixture of conductive and glass phase, observed mainly in ruthenate-based resistors.

After firing at 500°C, small, micrometer-sized particles, shown in Fig. 7a and at higher magnification in Fig. 7b, appeared on the surface of the 8029 resistors. EDS analysis showed that these particles are clusters of RuO_2 single crystals. Similar RuO_2 crystals could not be found either on the surface of the 8029 resistor paste which was dried at 150° or fired at temperatures higher than 500°C. This indicates that the RuO_2 is not present in the "original" resistor paste (note that the 8029 is based on bismuth ruthenate or lead-modified bismuth ruthenate) and is therefore formed during firing at 500°C. As this temperature is too low for softening and sintering of the glass phase and the resulting possible interactions between glass and ruthenate-based conductive phase, the formation of RuO_2 crystals is presumably due to the organic vehicle burn-out process. A possible explanation, given by Pierce *et al*. [24], is as follows: after drying, i.e. the evaporation of the solvent from the organic vehicle, the ruthenate particles are "dressed" in a layer of organic material. Even with an adequate supply of air in the furnace, the oxidation of organic material in the organic/conductive-particles composite is a relatively slow process, governed by the

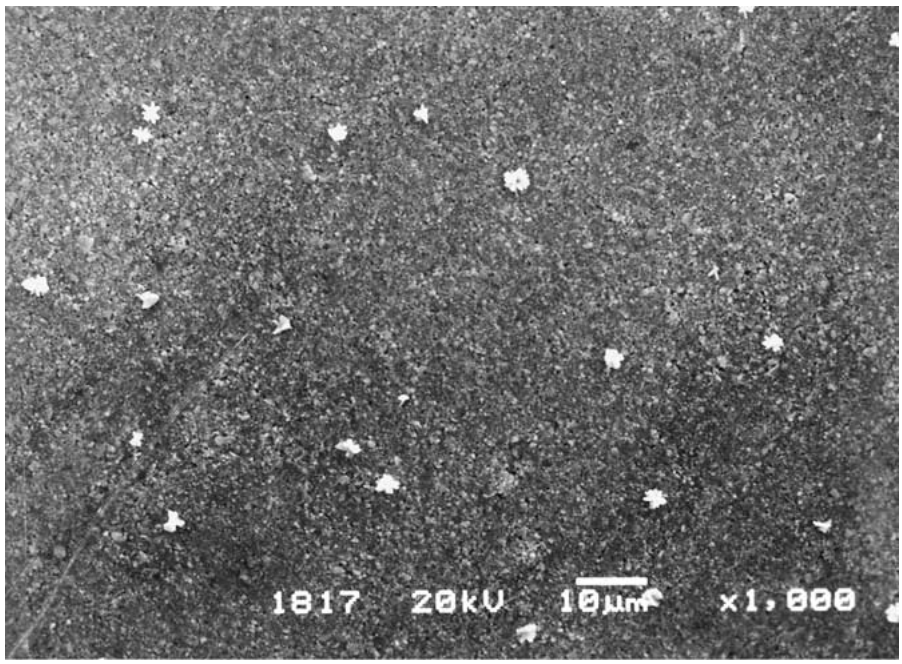

(a)

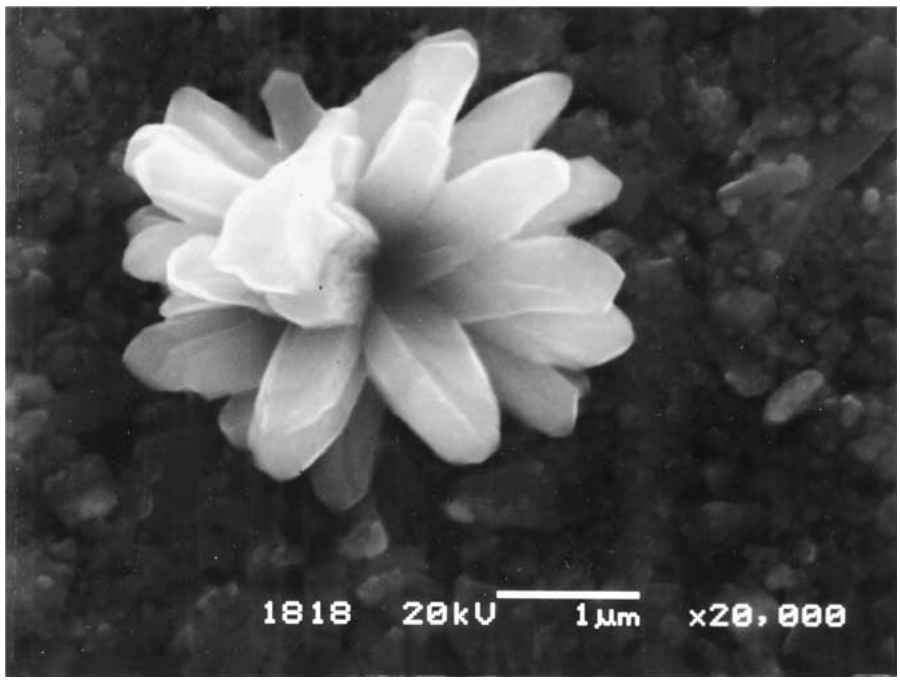

(b)

Figure 7 (a) Microstructure of thick-film resistor 8029, fired for 10 min at 500°C. After burn out the micrometer-sized particles appeared on the surface. (b) The cluster of RuO_2 single crystals, which appeared on the surface of thick-film 8029 resistor after firing at 500°C.

TABLE II Cold (−25°C to 25°C) and hot (25°C to 125°C) TCRs, relative sheet resistivities, and noise indices of resistors, fired at different temperatures

T firing (°C)	Resistor	Cold TCR ($\times 10^{-6}$/K)	Hot TCR ($\times 10^{-6}$/K)	Rel. resistivity (%)	Noise (dB)
600	2031	635	630	49	−9.7
	8029	−445	−445	32	−9.8
	8031	–	–	–	–
700	2031	330	330	84	−15.5
	8029	−45	−115	85	−19.1
	8031	−280	−195	2400	24.5
800	2031	95	105	94	−16.3
	8029	−65	0	129	−19.5
	8031	−130	−70	137	−12.3
825	2031	60	75	97	−19.3
	8029	−41	20	120	−19.3
	8031	−65	−10	111	−13.9
850	2031	35	45	100	−20.3
	8029	15	65	100	−18.1
	8031	5	50	100	−15.0
875	2031	10	20	102	−21.1
	8029	60	105	89	−17.1
	8031	60	80	105	−15.9
900	2031	−20	−15	103	−21.0
	8029	205	255	65	−17.1
	8031	50	100	105	−17.8
925	2031	−55	−50	107	−22.2
	8029	630	635	34	−18.5
	8031	60	110	106	−18.5
950	2031	−50	−50	100	−22.8
	8029	585	565	26	−19.1
	8031	75	130	104	−20.3

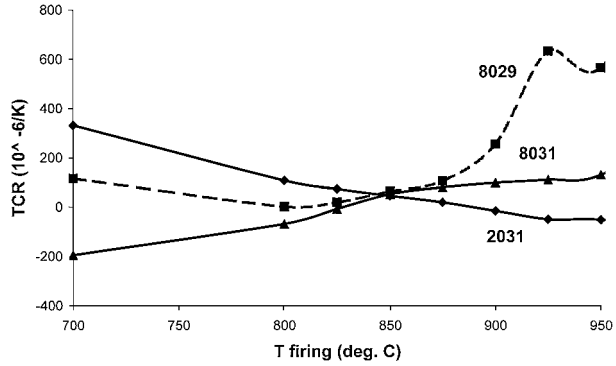

Figure 8 The dependence of hot TCRs (25°C to 125°C) vs. firing temperature for 8029, 8031 and 2031 thick-film resistors.

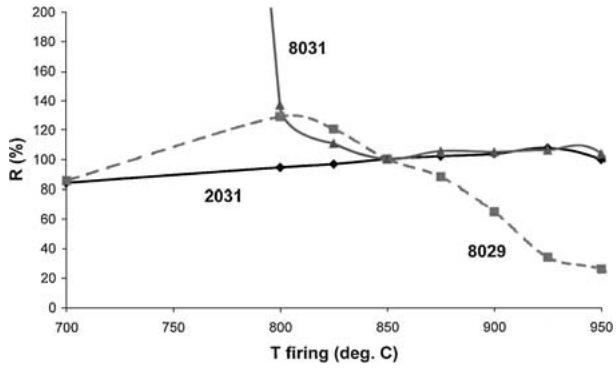

Figure 9 The dependence of relative sheet resistivities vs. firing temperature for 8029, 8031 and 2031 thick-film resistors.

diffusion of oxygen into the organic layer. The ruthenate particles could therefore be reduced to metallic ruthenium and Bi_2O_3 following the schematic equation (C─H stands for organic material):

$$Bi_2Ru_2O_7 + C{-}H\text{- - -} \rightarrow Bi_2O_3 + 2Ru + CO/CO_2 + H_2O \quad \text{(schematic equation)}$$

When all the organic material is burnt out, the finely divided ruthenium metal oxidises back to the ruthenium oxide, seen in Fig. 7. At higher firing temperatures these small single crystals disappear, probably forming ruthenate pyrochlore again, either due to the reaction with PbO from the glass phase or with Bi_2O_3 which was "left over" during reduction.

3.2. Electrical characterisation

The relative sheet resistivities of resistors fired at different temperatures, cold (−25°C to 25°C) and hot (25°C to 125°C) TCRs, and noise indices are shown in Table II. Relative sheet resistivities, given in percents, are based on the resistivities of resistors fired for 10 min at 850°C. Note, however, that the resistivities of all resistors fired at 500°C, as well as the resistivity of the 8031 fired at 600°C, are too high for measurement. The dependence of hot TCRs vs. firing temperature is also graphically presented in Fig. 8 and the dependence of relative sheet resistivities on firing temperature in Fig. 9.

TCRs of the 2031 resistors are positive for firing temperatures up to 875°C and negative for higher firing temperatures. TCRs of 8031 and 8029 resistors are negative for lower firing temperatures and became more positive for higher firing temperatures over 850°C. This tendency is more pronounced for the 8029 material, which reaches values around 600×10^{-6}/K at 950°C. The resistivity vs. temperature dependence of 8029, fired at 950°C, is almost linear. The calculated R-squared value is $R^2 = 0.999$, which is comparable to Pt based thick film resistors and thick film PTC resistors [25]. In general, the absolute values of cold and hot TCRs first decreased to a minimum after firing at 850°C and then increased again with increasing firing temperature. The TCRs of all resistors fired at the "normal" temperature of 850°C are well below 100×10^{-6}/K.

Sheet resistivities of the 2031 resistors are at first increasing slightly and at higher firing temperatures over 900°C decreasing slightly with increasing firing temperature. Sheet resistivities of the 8029 resistors are at first increasing and, after firing at 800°C, sharply decreasing with increasing firing temperature. After firing at 950°C the resistivity is only around 250 ohm/sq., i.e. around 25% of the nominal value. The resistivity of the 8031 samples is very high, around 20 kohm/sq., after firing at 700°C. The resistivity is then rather stable around its nominal value of 1 kohm/sq. for firing temperatures up to 950°C. Based on resistivity and TCR data, the electrical characteristics of the 2031 resistors seems to be the least influenced by the firing temperature over this wide temperature range.

The noise indices of the resistors, shown in Table II, where they are expressed in dB, are also graphically presented in Fig. 10, where the noise indices are expressed

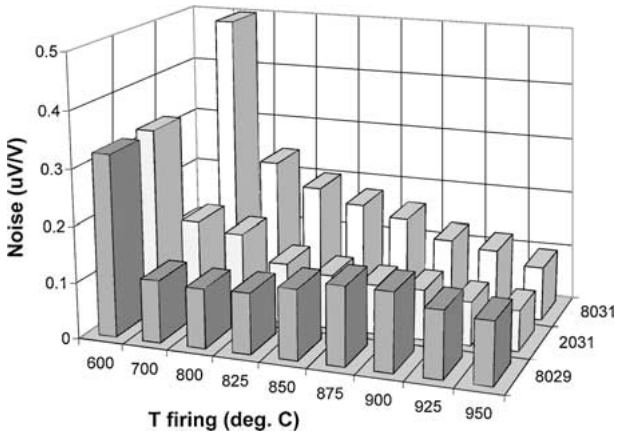

Figure 10 Noise indices of 2031, 8029 and 8031 resistors, fired at different temperatures.

in uV/V. Note that these two units are "connected" with a very simple equation:

$$\text{Noise (dB)} = 20 \times \log \text{noise (uV/V)}$$

The noise indices of resistors mostly decrease with increasing firing temperature. The exception is the 8029 resistors, where the noise index slightly increases at firing temperatures between 800°C and 950°C. Note, however, that the noise index of the 8031 resistor, fired at 700°, which also has a very high sheet resistivity, is very high, around 17 uV/V (25 dB). As the scale of the noise in Fig. 10 is adjusted to 0.5 uV/V the value of the 8031 resistor noise index is cut off. When resistors are fired at the "normal" firing temperature of 850°C, the 2031 resistors have the lowest noise, below 0.1 uV/V (−20 dB).

4. Conclusions

The microstructural and electrical characteristics of three 1 kohm/sq. thick-film resistor pastes, based on RuO_2 (8031) ruthenate (8029) or a mixture of both conductive phases (2031), fired at temperatures between 500°C and 950°C, were investigated. The cell parameters of RuO_2 in 8031 and 2031 resistors, bismuth ruthenate in 8029 resistors and lead ruthenate in 2031 resistors, were calculated from X-ray data. The calculated cell dimensions of the cubic bismuth ruthenate in 8029 resistors are smaller than the cell parameters reported in the literature while the dimensions of lead ruthenate in 2031 resistors are larger.

The microstructure of fired 8031 resistors, based on RuO_2, consists of "chains" of conductive clusters (very small RuO_2 particles embedded in glass) around glass "islands" while the microstructure of ruthenate-based 8029 resistors, and the RuO_2 and the ruthenate-based 2031 resistor is a mixture of conductive particles and glass phase. After firing at 500°C, small, micrometer-sized clusters of RuO_2 single crystals appeared on the surface of the 8029 resistors. At higher firing temperatures RuO_2 crystals disappeared, presumably due to a reaction with the glass phase.

The absolute values of cold and hot TCRs first decreased to a minimum at 850°C and then increased with increasing firing temperature. The sheet resistivity of the 2031 material is at first increasing to some extent and at higher firing temperatures over 900°C decreasing slightly with increasing firing temperature. The sheet resistivity of the 8029 material is at first increasing and, above a firing temperature of 800°C, sharply decreasing with increasing firing temperature and reaches around 25% of the nominal value after firing at 950°C. The resistivity of the 8031 material is very high after firing at 700°C. At higher firing temperatures the resistivity is rather stable around its nominal value of 1 kohm/sq. for firing temperatures up to 950°C. The noise indices of resistors generally decrease with increasing firing temperature. The exceptions are the 8029 resistors, where the noise indices slightly increase at firing temperatures between 800°C and 950°C. Based on resistivity, TCR, and noise indices data, the electrical characteristics of the 2031 resistors, when compared with the other two materials, seems to be the least influenced by firing temperature over this wide temperature range.

Acknowledgement

The authors wish to thank Mr. Mitja Jerlah (HIPOT) for printing and firing the test circuits as well as TCR and noise measurements. The financial support of the Ministry of Science and Technology of Slovenia is gratefully acknowledged.

References

1. R. W. VEST, *Ceram. Bull.* **65**(4) (1986) 631.
2. T. INOKUMA and Y. TAKETA, *Active and Passive Elect. Comp.* **12**(3) (1987) 155.
3. O. ABE, Y. TAKETA and M. HARADOME, *ibid.* **13**(2) (1988) 76.
4. M. PRUDENZIATI, B. MORTEN and A. MASEORO, *J. Phys. D; Appl. Phys.* **14**(7) (1981) 1355.
5. K. ADACHI, S. IIDA and K. HAYASHI, *ibid.* **9**(7) (1994) 1866.
6. J. LEE and R. W. VEST, *IEEE Trans. Components, Hybrids, and Manufacturing Tecnology* **CHMT-6**(4) (1983) 430.
7. A. KUBOVY and I. HAVLAS, *Ceramics–Silikaty* **32**(2) (1988) 109.
8. T. YAMAGUCHI and K. IIZUKA, *J. Amer. Ceram. Soc.* **73**(7) (1990) 1953.
9. M. HROVAT and F. JAN, *Hybrid Circuits* **14** (1987) 25.
10. B. MORTEN, M. PRUDENZIATI, M. SACHI and F. SIROTTI, *J. Appl. Phys.* **63**(7) (1988) 2267.
11. B. MORTEN, A. MASOERO, M. PRUDENZIATI and T. MANFREDINI, *J. Phys. D: Appl. Phys.* **27**(10) (1994) 2227.
12. A. T. WALKER, L. A. SILVERMAN, K. W. HANG, T. PFEITFER, V. P. SIUTA, L. H. SLACK and R. J. BOUCHADR, in Proc. Int. Symp. Microelectronics ISHM-93, Dallas, November 1993, p. 695.
13. P. O'CALLAGHAN, A. T. WALKER, K. W. HANG, V. P. SIUTA, J. J. OSBORNE, J. SMITH, K. HAYAKAWA and A. BUCKTHORPE, *Microelectronics Int.* **37** (1995) 14.
14. M. HROVAT, Z. SAMARDŽIJA, J. HOLC and D. BELAVIČ, *J. Mater. Sci.: Materials in Electronics* **11**(3) (2000) 199.
15. MIL—STD 202B, Method 308.
16. K. ADACHI and H. KUNO, *J. Amer. Ceram. Soc.* **80**(5) (1997) 1055.
17. R. J. BOUCHARD and L. J. GILLSON, *Mater. Res. Bull.* **6**(8) (1971) 669.

18. M. A. SUBRAMANIAN, G. ARAVAMUDAN and G. V. S. RAO, *Progress in Solid State Chem.* **24** (1981) 55.
19. H. S. HOROWITZ, J. M. LONGO and J. T. LEWANDOWSKI, *Mater. Res. Bull.* **16**(5) (1981) 489.
20. M. SCHULER and S. KEMMLER-SACK, *J. Less-Common Metals* **102** (1984) 105.
21. T. V. NORDSTROM and C. R. HILLS, in Proc. Int. Hybrid Microelectronics Symp. ISHM-79, Los Angeles, 1979, 40.
22. A. KUBOVY, *J. Phys. D: Appl. Phys.* **19** (1986) 2127.
23. M. HROVAT, G. DRAŽIČ, J. HOLC and D. BELAVIČ, *J. Mater. Sci. Lett.* **14**(15) (1995) 1048.
24. J. W. PIERCE, D. W. KUTY and J. R. LARRY, *Solid State Technol.* **25**(10) (1982) 85.
25. M. HROVAT, D. BELAVIČ and Z. SAMARDŽIJA, *J. Mater. Sci. Lett.* **19**(8) (2000) 651.

Received 12 April 2001
and accepted 7 February 2002